Correlation analysis for energy losses, waiting times and durations of type I edge-localized modes in the Joint European Torus

A.Shabbir[1,2], G.Verdoolaege[1,3], G.Hornung[1], O.J.W.F. Kardaun[2], H.Zohm[2] and JET contributors ‡

EUROfusion Consortium, JET, Culham Science Centre, Abingdon, OX14 3DB, UK
[1]Department of Applied Physics, Ghent University, B-9000 Ghent, Belgium
[2]Max Planck Institute for Plasma Physics, D-85748 Garching, Germany
[3]Laboratory for Plasma Physics, Royal Military Academy, B-1000 Brussels, Belgium

E-mail: aqsa_shabbir@outlook.com

Abstract. Several important ELM control techniques are in large part motivated by the empirically observed inverse relationship between average ELM energy loss and ELM frequency in a plasma. However, to ensure a reliable effect on the energy released by the ELMs, it is important that this relation is verified for individual ELM events. Therefore, in this work the relation between ELM energy loss (W_{ELM}) and waiting time (Δt_{ELM}) is investigated for individual ELMs in a set of ITER-like wall plasmas in JET. A comparison is made with the results from a set of carbon-wall and nitrogen-seeded ITER-like wall JET plasmas. It is found that the correlation between W_{ELM} and Δt_{ELM} for individual ELMs varies from strongly positive to zero. Furthermore, the effect of the extended collapse phase often accompanying ELMs from unseeded JET ILW plasmas and referred to as the slow transport event (STE) is studied on the distribution of ELM durations, and on the correlation between W_{ELM} and Δt_{ELM}. A high correlation between W_{ELM} and Δt_{ELM}, comparable to CW plasmas is only found in nitrogen-seeded ILW plasmas. Finally, a regression analysis is performed using plasma engineering parameters as predictors for determining the region of the plasma operational space with a high correlation between W_{ELM} and Δt_{ELM}.

Keywords: edge-localized mode (ELM), correlation analysis, JET, waiting times

1. Introduction

Standard high confinement (H-mode) regimes in tokamaks are characterized by the existence of an edge transport barrier (ETB) (typically called pedestal) in a narrow edge region inside the separatrix. Steep pressure gradients in the ETB lead to

‡ See the Appendix of F. Romanelli et al., Proceedings of the 25th IAEA Fusion Energy Conference 2014, Saint Petersburg, Russia.

magnetohydrodynamic (MHD) instabilities called the *edge-localized modes* (ELMs) [1][2]. ELMs are intense, short duration, repetitive events that cause a partial collapse of the ETB and result in sudden expulsion of energy and particles from the plasma edge. On the one hand, ELMs pose a serious concern as they can cause high transient heat loads on the plasma-facing components (PFCs) [3]. On the other hand, they are crucial for regulating the core concentration of impurities, in particular, tungsten (W), which is produced by plasma- wall interactions at the divertor target. Paradoxically, ELMs are required for impurity flushing even though they are responsible for at least a fraction of the W production in H-mode plasmas. Larger ELMs in terms of ELM energy loss (W_{ELM}) have been found to give a larger W source per ELM [4].

Given the importance of ELMs for the successful operation of next-step fusion devices, a large array of ELM control and mitigation techniques have emerged [3][5]. Typically, ELM losses are influenced either by a complete suppression of the ELMs in regimes where an alternate mechanism replaces the energy and particle transport, or by increasing the ELM frequency (f_{ELM}) over its natural value (*ELM pacing*), so that the ELM losses become smaller. The effectiveness of the latter method in reducing the peak ELM energy flux (q_{max}) at the ITER divertor may be dampened in the wake of the experimentally observed linear dependence of the effective ELM energy deposition area (A_{ELM}) on ELM size (W_{ELM}) [6] [7][8][9]. §

However, Loarte *et al.* [10] notes, that while the broadening of A_{ELM} certainly expands the operational regime of uncontrolled ELMs, for conditions in which the uncontrolled ELMs would exceed the limits posed by divertor erosion, ELM control will be necessary at ITER. Secondly, the processes that lead to the broadening of A_{ELM} at the divertor will also have a similar effect on the scrape-off layer (SOL). This will inevitably result in an increase in the energy deposited on ITER's main wall which will consist of Beryllium (Be) PFCs. Be in contrast to the divertor material W, has a much lower erosion threshold which makes it highly likely that for some conditions the erosion limit of the first wall could constrain uncontrolled ELM operation.

Further, the recent ELM pacing experiments at DIII-D using lithium granules in contrast to frozen deuterium pellets, report on a reduction of the q_{max} at the outer strike point [11]. This result not only suggests the possibility of reducing q_{max} at ITER by non-fuel pellet injection but also presents an added advantage of de-coupling ELM pacing from plasma fueling.

Furthermore, in addition to the protection of PFCs, ELM control requirements at ITER have been recently revised to include W impurity control [12][10]. Excessive W concentration in the core can lead to severe central radiation losses which can affect the H-mode performance and in extreme cases result in a radiative collapse [13]. Experimental observation at JET [14] and AUG [15] have shown that a sufficiently high f_{ELM} will be required in ITER for maintaining an appropriate W concentration in the plasma.

§ We here mention also recent work concerning the multi-machine scaling of ELM heat loads deposited at the divertor [Eich PSI 2016].

ELM pacing [16][17], a leading candidate for controlling (W_{ELM}) in ITER, relies on the observed inverse dependence of W_{ELM} on f_{ELM}. For type I ELMs, using a multi-machine database and a wide range of plasma parameters averaged over multiple ELM events it has been empirically found that [18],

$$\bar{W}_{ELM} = 0.2 W_{plasma} \left(\frac{\bar{\Delta} t_{ELM}}{\tau_E} \right). \tag{1}$$

Here, τ_E is the energy confinement time in plasmas with a stored energy W_{plasma} and $\bar{\Delta} t_{ELM}$ is the average period of the ELM cycle ($\bar{\Delta} t_{ELM} = 1/f_{ELM}$). ELM control methods exploit a similar inverse dependence between f_{ELM} and energy loss by increasing the f_{ELM} significantly beyond the natural frequency, leading to smaller ELM energy losses.

As ELM events are repetitive and not periodic, $\bar{\Delta} t_{ELM}$ is customarily estimated as

$$\bar{\Delta} t_{ELM} = \frac{1}{N} \sum_{i=1}^{N} \Delta t_{ELM_i}. \tag{2}$$

Here Δt_{ELM_i} is the time since the previous ELM and is also frequently referred to as the *waiting time* of ELM i. In this work, in contrast to analyzing the relation of the averages, the relation between Δt_{ELM_i} and W_{ELM} for individual type I ELMs is investigated in a set of JET plasmas with PFCs made of carbon fiber composites (hereafter carbon-wall or CW) and ITER material combination (Be and W) (hereafter ITER-like wall or ILW). In an earlier investigation, Webster *et al.* [19] observed that the inverse dependence between W_{ELM} and f_{ELM} is not obeyed by individual ELMs for Δt_{ELM} greater than $20ms$. However, their analysis was restricted to a set of 2 T, 2 MA type I ILW plasmas from the JET tokamak. In this work, the analyzed plasmas are selected to cover a wide range of plasma parameters in JET. The aim is to show that an inversely linear relation similar to (1) is obeyed in some plasmas, but not all. The correlation between Δt_{ELM} and W_{ELM} is seen to vary in CW discharges and it is usually low in ILW plasmas, except when nitrogen is seeded into the plasma. This is further investigated by examining the relation between ELM durations (τ_{ELM}) and W_{ELM}, as well as the correlation between energies of consecutive ELMs. This includes a comparative analysis between ILW and CW plasmas. A weak or no relation between waiting times and ELM energies could adversely affect the potential of ELM control methods. Therefore, the present work also aims to emphasize the importance of considering the probability distribution of stochastic plasma quantities (in this case Δt_{ELM} and W_{ELM}), as it contains more information compared to a mere average.

Finally, with the aim to locate regions of the machine operational space where ELM control would have a reliable effect on ELM energies, a regression analysis is performed of the correlation between Δt_{ELM} and W_{ELM} on several global plasma parameters.

The structure of the paper is as follows. In section 2, we describe the dataset as well as the estimation of the ELM characteristics Δt_{ELM}, W_{ELM} and τ_{ELM}. We also present the statistical tools that are used to assess the strength of the relation between the various parameters of interest. In section 3, first the relation between the

Table 1. Range of some key global plasma parameters for the JET ILW, JET CW and the six N_2-seeded JET ILW plasmas analysed in this work.

		CW	ILW	ILW (N_2 seeded)
No. of discharges	M	20	32	6
No. of ELMs per discharge	N	65 ± 30	70 ± 30	60 ± 20
Toroidal field	$B_t(T)$	1.6 - 3.0	1.3 - 2.7	2.65 - 2.7
Plasma current	$I_p(MA)$	1.5 - 3.0	1.3 - 2.5	2.5
Line-integrated edge density	$n_e(10^{19}m^{-2})$	3.2 - 9.9	1.9 - 7.4	5.4 - 7.4
Input power = $P_{ohmic} + P_{NBI}$	$P_{input}(MW)$	8.1 - 22	6.9 - 19	16 - 19
Main gas (D_2) flow rate	$\Gamma_{D_2}(10^{22}s^{-1})$	0.0 - 7.5	0.52 - 4.0	1.3 - 3.7
(N_2) flow rate	$\Gamma_{N_2}(10^{22}s^{-1})$	-	-	0.76 - 2.8
Average triangularity	δ_{avg}	0.27 - 0.43	0.27 - 0.41	0.27 - 0.39
Edge safety factor	q_{95}	2.8 - 3.6	3.1 - 6.1	3.4
Beta normalized	β_N	1.6 - 2.4	0.92 -2.0	1.2 - 1.7

average quantities is investigated, followed by a similar analysis on the same quantities for individual ELMs in a specific discharge. We then study the picture that emerges when all individual ELMs from our database are analyzed together. This is followed by regression analysis of the correlation between waiting times and energy losses, as a function of machine parameters in section 4. Finally, in Section 5 we analyze W_{ELM} of consecutive ELMs before concluding the work in section 6.

2. Database and methods for correlation analysis

2.1. Plasma scenario

For this investigation, an intermediate-size database of 20 CW and 32 ILW JET plasmas has been compiled. We call this database "JET ELMy database (DBII)", henceforth referred as JET ELM-DBII. The dataset has been selected with a view on encompassing a relatively wide range of plasma and engineering parameters. Each selected discharge has a steady period of H-mode with regular type I ELMs and the analysis has been restricted to time intervals where plasma conditions are quasi-stationary. To ensure quasi-stationarity, it has been regarded essential that in the analyzed time interval of approximately 2.5 - 3 seconds, the plasmas have approximately constant gas fueling, input power, edge density and β_N. The size of the current database has somewhat been restricted by the necessary level of manual intervention for extracting data and in part due to the required availability of signals with a sufficient temporal resolution. However, the current size of the database is adequate for the analysis carried out in this work.

With the replacement of CW in JET by the ILW in 2010, it has been observed that the first wall material appears to have had an effect on both the plasma confinement and pedestal properties [20][21]. Up until now, the JET-ILW standard baseline scenario has not routinely achieved a confinement factor of $H_{98} = 1$ both in low and high-triangularity scenarios. The degraded confinement in JET ILW plasmas is a result of a lower pedestal

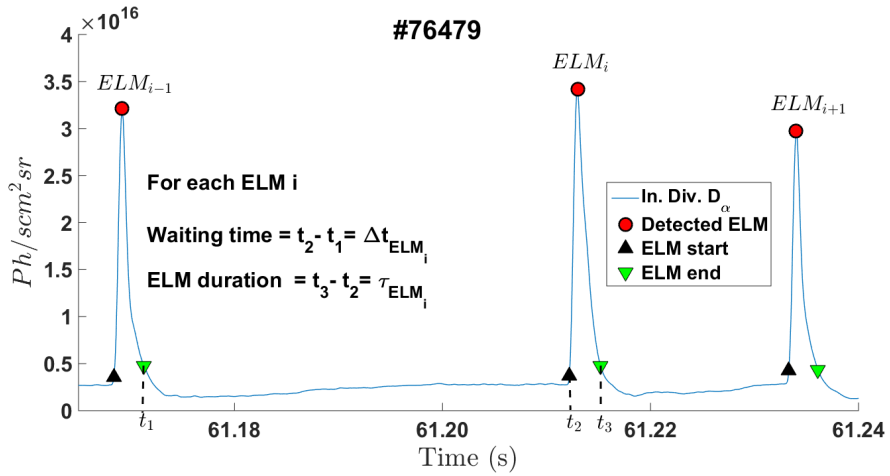

Figure 1. Illustration of the extraction of ELM waiting times (Δt_{ELM}) and ELM durations (τ_{ELM}) from a time trace of D_α radiation at JET's inner divertor.

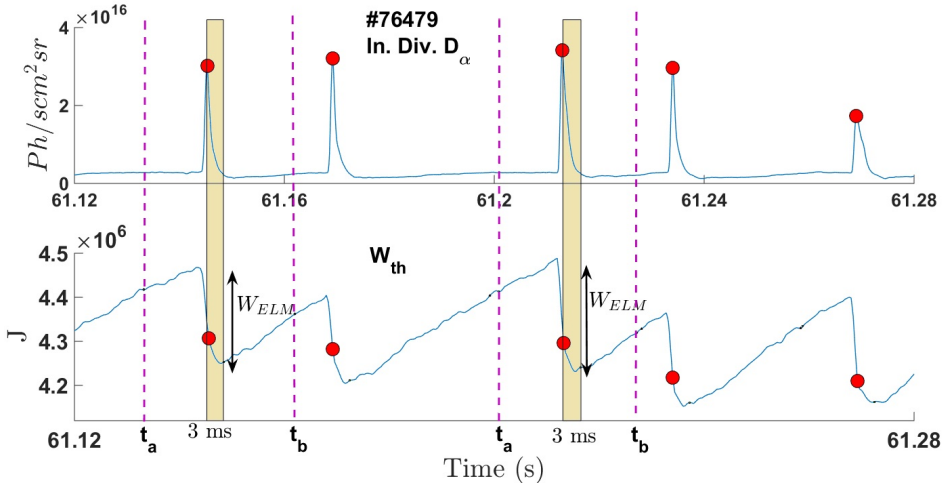

Figure 2. Illustration of ELM energy loss (W_{ELM}) estimation from the equilibrium stored energy (W_{MHD}), synchronized to the time trace of D_α radiation at JET's inner divertor.

pressure mainly due to a pedestal temperature approximately 20-30 percent lower than in JET CW. Pedestal density on the other hand is comparable among JET CW and JET ILW plasmas. In JET ILW a pedestal pressure comparable to baseline JET CW has only been achieved in high-triangularity experiments with nitrogen (N_2) seeding [21][24]. In the current work, 6 ILW plasmas with N_2 seeding are also included in the dataset, making the total number of analyzed ILW plasmas 38. The range of a number of important engineering parameters in the database is given in table 1.

2.2. ELM detection and energy loss estimation

A robust threshold-based algorithm has been developed for estimating ELM temporal properties, that is Δt_{ELM} and τ_{ELM}. The algorithm examines Balmer alpha radiation

from Deuterium (D_α) for the CW plasmas and Beryllium II (527 nm) radiation for ILW plasmas at JET's inner divertor. The algorithm uses the sharp spikes in D_α/Be II radiation for detecting ELMs. This is preceded by a smoothing process of the time traces and is followed by a threshold-based detection of ELM start and end times. The estimation of Δt_{ELM} and τ_{ELM} is illustrated in figure 1. The ELM energy loss has been estimated from the high-resolution time-resolved measurement of the equilibrium stored energy (W_{MHD}). W_{MHD} is calculated by plasma boundary and pressure reconstruction, assuming constant pressure on magnetic surfaces. The W_{MHD} time trace is synchronized to individual ELMs and W_{ELM} is estimated as the maximum loss in energy in a small time window around an ELM event. This is illustrated in figure 2. The time window (delimited by t_a and t_b) is chosen dynamically, with t_a taken as 3/4 of the time till the next ELM and t_b taken as 1/3 of the time since the last ELM. Dynamic selection of the time window compensates for the varying timescales of ELM energy loss between JET CW and JET ILW plasmas [22]. Furthermore, in order to offset inaccuracy arising due to eddy currents in the vacuum vessel and small radial plasma motion following an ELM, a time interval of 3 ms has been allowed after an ELM in which the data is not used for energy loss estimation.

2.3. ELM duration and slow transport events

JET ITER-like wall ELMs are sometimes followed by an extended collapse phase, called the *slow transport event* (STE) [22], the presence of which has been proposed to be related to divertor/scrape-off layer (SOL) conditions [23] [24] and to a change in recycling behavior in a W divertor [25] [26] . These STEs are analogous to the second phase of ELM collapse observed at ASDEX Upgrade (AUG) [24]. The typical temporal signature of an STE is shown in figure 3(a) and 3(b). The corresponding W_{ELM} are shown in 3(d)-(f). ELMs accompanied by an STE have longer time scales of temperature and density collapse and result in higher total energy loss of the plasma than the losses produced by ELMs alone. We first studied the variation of the energy released by an ELM, averaged over all ELM events in a single discharge, in terms of the fraction of STEs. The latter is defined as

$$f_{STE} = \frac{N_{(ELM+STE)}}{N_{ELM} + N_{(ELM+STE)}}, \tag{3}$$

where $N_{(ELM+STE)}$ is the number of ELMs accompanied by a slow transport event and N_{ELM} is the number of ELMs that are not followed by an STE phase, hereafter referred to as pure ELMs. The ELM energy loss averaged over a single discharge, during stationary conditions, is denoted as $\bar{W}_{ELM}$ and we also consider its ratio w.r.t. $\bar{W}_{tot}$, i.e. the total stored equilibrium energy in the plasma, also averaged over the entire stationary phase of each discharge that has been investigated. The variation of $\bar{W}_{ELM}$ and $\bar{W}_{ELM}/\bar{W}_{tot}$ with the fraction of STEs (f_{STE}) for all plasma pulses is plotted in figure 4. In this work, we have divided JET ILW plasmas (M discharges) into three broad categories: those with a high fraction of STEs ($f_{STE} \geq 50\%, M = 4$), medium

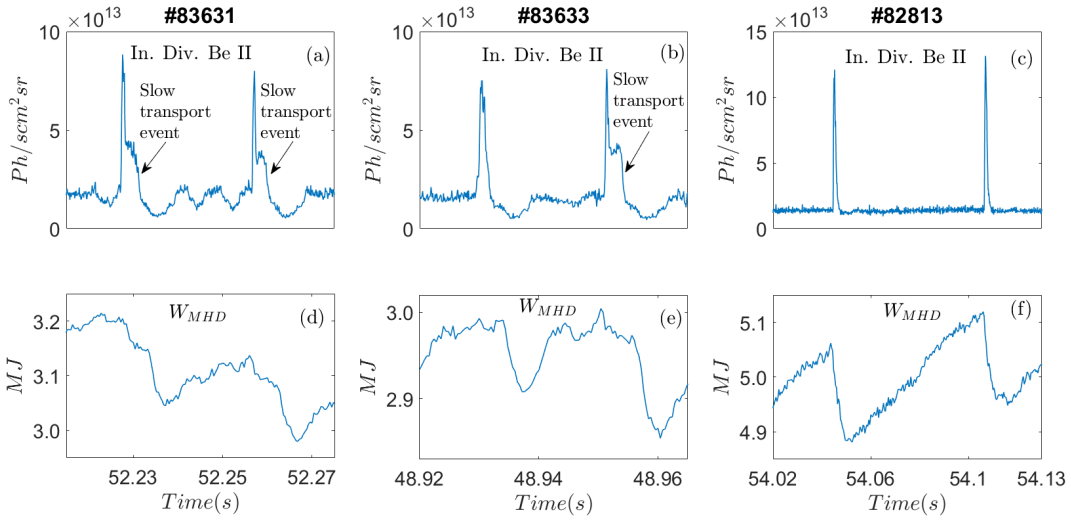

Figure 3. (a)-(c)Temporal signature of pure ELMs and ELMs followed by a slow transport event (STE) in three typical JET ILW plasmas. The N_2-seeded plasmas, like CW plasmas, have narrower ELMs and no slow transport events. (d)-(f) ELM energy loss (W_{ELM}) for the pure ELMs and ELMs followed by an STE shown in (a)-(c).

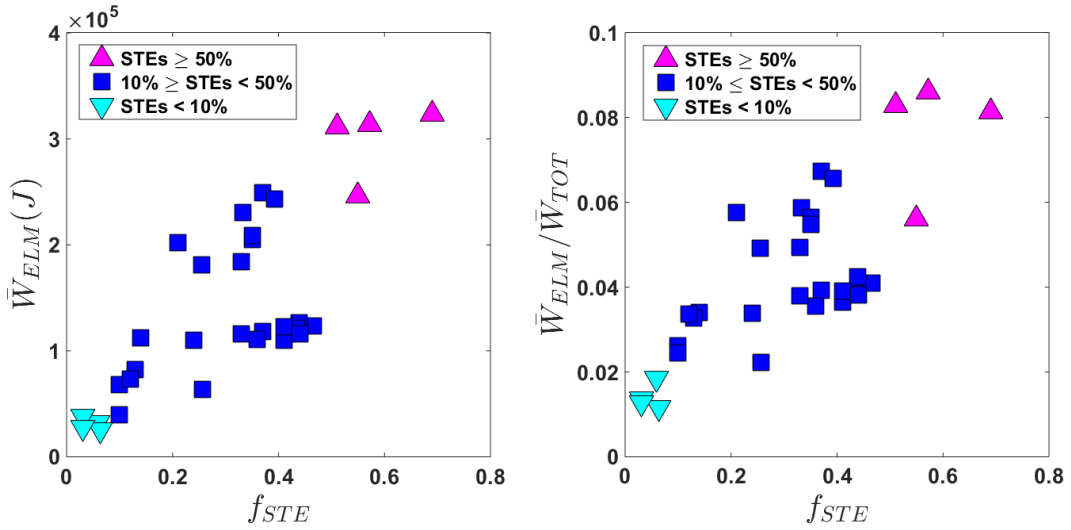

Figure 4. Variation of the mean ELM energy loss ($\bar{W}_{ELM}$) and mean relative ELM energy loss ($\bar{W}_{ELM}/\bar{W}_{tot}$) with the fraction of slow transport events (f_{STE}) in JET ILW plasmas.

fraction of STEs ($10\% \leq f_{STE} < 50\%, M = 24$) and those with very few or no STEs ($f_{STE} < 10\%, M = 4$). From figure 4, a clear (linear) increase can be noticed of $\bar{W}_{ELM}$ with the fraction of STEs in a plasma. A very similar conclusion is true for the relative energy loss $\bar{W}_{ELM}/\bar{W}_{tot}$, which shows that an increased energy loss is due to a higher fraction of STEs. This is in accordance with recent studies wherein it was seen that the STEs carry a significant proportion of the energy of the total ELM event [22]. STEs are absent in the JET CW database analyzed in this work. Furthermore, they

disappear in N_2-seeded ILW JET plasmas [22], as does the second part of the ELM collapse in AUG plasmas [24]. JET ILW ELMs, compared to JET CW plasmas have larger ELM durations (τ_{ELM}). This too, in a large part, is due to the existence of STEs in ILW plasmas. The average duration $\bar{\tau}_{ELM}$ of all ELM events during a period of stationary plasma conditions, for the plasmas analyzed in this work, are listed in table 2. N_2-seeded ILW plasmas and ILW plasmas with low f_{STE} have $\bar{\tau}_{ELM}$ similar to CW plasmas. ILW plasmas with high f_{STE} exhibit $\bar{\tau}_{ELM}$ about three times larger than the $\bar{\tau}_{ELM}$ of CW plasmas. An investigation into the distribution of τ_{ELM} yields that the non-seeded JET ILW plasmas (high f_{STE}) have a distribution of τ_{ELM} which is distinctly different from N_2-seeded JET ILW plasmas and JET CW plasmas. The latter two cases exhibit similar distributions for τ_{ELM}. Figure 5 (a)-(c) present the distribution of τ_{ELM} for non-seeded JET ILW plasmas (high f_{STE}), N_2-seeded JET ILW plasmas and JET CW plasmas. The distribution of τ_{ELM} for non-seeded JET ILW plasmas (high f_{STE}) is bimodal (two local maxima). The bimodal distribution arises as a mixture of two underlying unimodal distributions emerging from collapses due to pure ELMs and collapses followed by STEs. We performed a manual separation of pure ELM events from the cases with STEs, and the corresponding unimodal distributions are shown in figure 5(d) and (e), respectively. The pure ELMs have a duration τ_{ELM} that is typically less than about 5 ms, while the ELMs with STEs can last up to 14 ms. The distribution of τ_{ELM} for pure ELMs in high f_{STE} ILW plasmas (figure 5(d)) appear similar to the distribution of τ_{ELM} for N_2-seeded JET ILW plasmas (figure 5(b)) and JET CW plasmas (figure 5(c)). These distributions are visibly non-Gaussian with a strong positive skew and we verified that a similar degree of skewness also exists in the distribution of ELM durations from individual discharges. From the physical point of view it means that, in our data set, pure ELMs with durations longer than 4 - 5 ms are relatively rare, compared to the prevailing duration of about 2.5 ms. From the statistical point of view, characterization of skewed distributions necessitates additional metrics such as median and mode. The means and standard deviations alongside medians, and skewness estimates for each distribution are summarized in table 3. Here, the skewness was estimated not from the third-order moment of the distribution (which typically requires a lot of data points), but by dividing the difference between mean and median

Table 2. Typical ELM durations (mean ($\bar{\tau}_{ELM}$) and standard deviation ($std(\tau_{ELM})$)) for unseeded JET ILW plasmas (varying degrees of slow transport events), N_2-seeded JET ILW plasmas and JET CW plasmas.

	$\bar{\tau}_{ELM}(ms)$	$std(\tau_{ELM})(ms)$
ILW		
$f_{STE} \geq 50\%$	7.1	3.8
$10\% \leq f_{STE} < 50\%$	3.4	2.2
$f_{STE} < 10\%$	2.7	0.8
N_2-seeded	2.5	0.8
CW	2.6	1.2

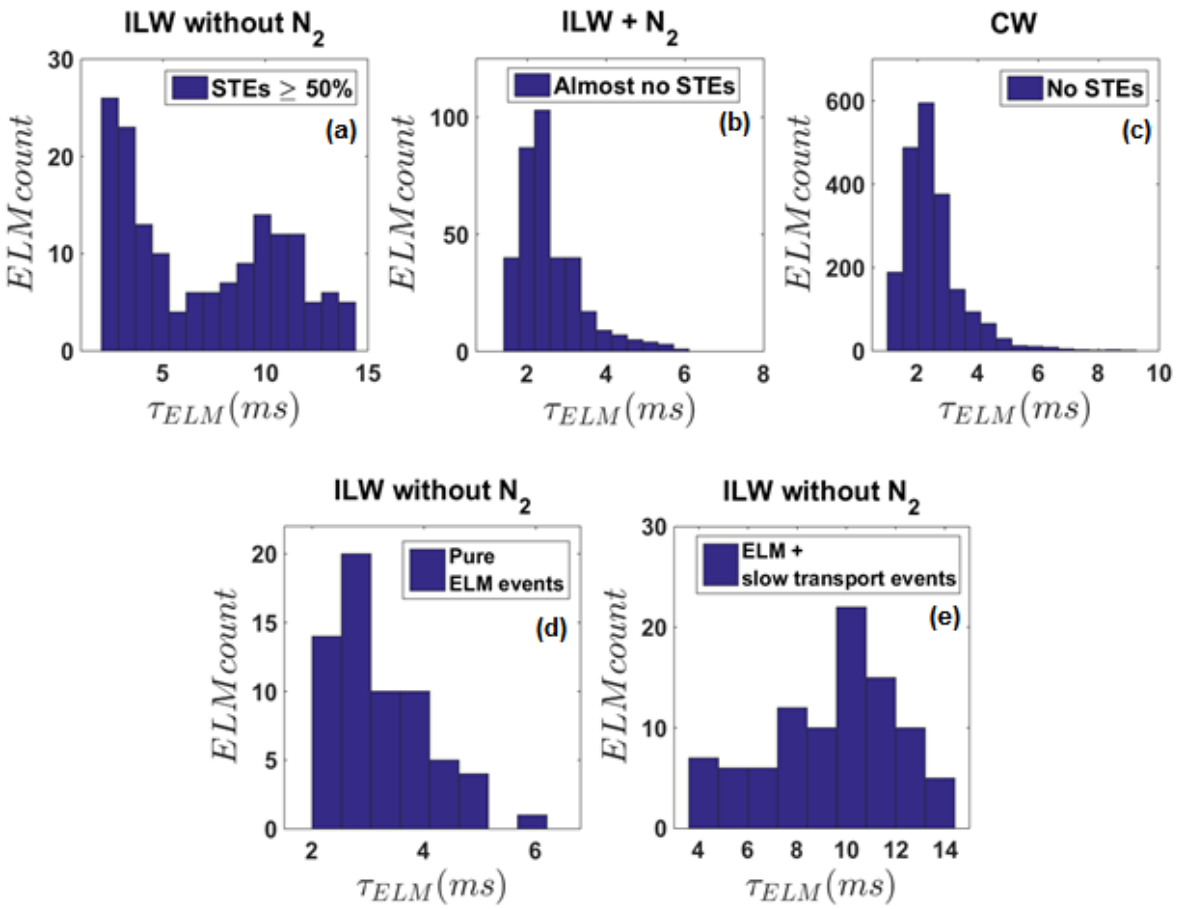

Figure 5. Distribution of ELM durations for various subsets of JET plasmas investigated in this work. In each panel, the vertical axis shows the number of ELM events. (a) Unseeded ILW plasmas with a high f_{STE}, (b) N_2-seeded ILW plasmas, (c) CW plasmas, (d) Pure ELMs from high f_{STE} unseeded ILW plasmas, (e) ELMs followed by $STEs$ from high f_{STE} unseeded ILW plasmas.

Table 3. Summary (mean ($\bar{\tau}_{ELM}$), standard deviation ($std(\tau_{ELM})$), median ($\tilde{\tau}_{ELM}$) and skewness) for the distributions of ELM durations extracted from the JET discharges investigated in this work.

JET plasmas		$\bar{\tau}_{ELM}$ (ms)	$std(\tau_{ELM})$ (ms)	$\tilde{\tau}_{ELM}$ (ms)	Skewness
ILW plasmas	Pure ELMs	3.2	0.87	3.0	0.23
$f_{STE} \geq 50\%$	ELMs + STEs	9.6	2.5	9.8	0.08
N_2-seeded ILW plasmas		2.5	0.81	2.3	0.25
CW plasmas		2.6	1.2	2.3	0.25

with standard deviation. For gaining an interesting insight into skewness estimation, the reader may refer to [27]. Contrary to pure ELM events, the distribution of τ_{ELM} for ELMs followed by STEs in high f_{STE} JET ILW plasmas (figure 5(e)) follows a more symmetric distribution.

2.4. Tools for correlation analysis

For analyzing the relation between ELM waiting times and energy losses, as a first step we use scatter graphs to get a qualitative impression. Furthermore, in order to quantify the strength of linear relation between Δt_{ELM} and W_{ELM} for individual ELMs within single discharges, the regular Pearson's product moment correlation coefficient (ρ) is estimated. Background theory can be found in [28][29][30] [31]. Herein, we present a brief simplified summary tailored to our limited needs.

For two related sets of data that can be modeled as outcomes of random variables X and Y, this correlation coefficient is defined as,

$$\rho_{X,Y} = \frac{cov(X,Y)}{\sigma_X \sigma_Y}, \tag{4}$$

where *cov* stands for the covariance between the variables, while σ_X and σ_Y are their standard deviations. The coefficient $\rho_{X,Y}$ takes values in the range $[-1, 1]$; a value of 1 means that X and Y are perfectly linearly correlated, a value of 0 that there is no correlation, while a value of -1 that they are perfectly anti-correlated.

Further statistical inference that we will perform in various situations, based on the estimates of ρ include estimation of confidence intervals, testing the significance of correlations and regressing against a set of global engineering parameters. This is complicated by the fact that the standard estimate of ρ has a non-Gaussian distribution. Therefore estimates r of ρ are converted to a z-value, the approximate distribution of which has been well investigated for a bivariate normal parent distribution:

$$z \equiv \frac{1}{2} \ln \frac{(1+r)}{(1-r)} = \tanh^{-1}(r). \tag{5}$$

For reasonable sample sizes, the mean of the distribution is close to the z-value itself, while the standard deviation does not notably depend on ρ and can be approximated by $\sigma_z = 1/\sqrt{n-1}$, where n is the number of data points. For non-normal parent distribution, the distribution of z is more complicated, see [31].

Further, we follow standard hypothesis test procedures [30] in testing the significance of correlation r. First, we specify the null (H_o) and alternative (H_A) hypotheses:

$$H_o : \rho = 0$$

$$H_A : \rho \neq 0$$

Under the hypothesis $\rho = 0$, the following test statistic t is known to follow a Student-t distribution with $N-2$ degrees of freedom,

$$t = r\sqrt{\frac{n-2}{1-r^2}} \tag{6}$$

Given that the null hypothesis is true, the probability ('p-value') of obtaining a value as large as t or greater is determined. If the p-value is smaller than the pre-set significance level α, the null hypothesis is rejected and ρ is deemed to be significantly different from

zero. The value of α is customarily taken as 0.05 and occasionally, especially for large sample sizes (say n between 100 and 1000), more stringently as 0.01.

In addition, we use an alternative measure of correlation, known as Spearman's rank correlation coefficient r_s, which measures monotonic dependence between X and Y:

$$r_s = 1 - \frac{6\sum_{i=1}^{n}(X_i - Y_i)^2}{n(n^2-1)}, \tag{7}$$

where X_i denotes the rank of the value X_i in the ordered series of values of the variable X. The estimate r_s is a nonparametric measure of dependence and compared to r is much less sensitive to outliers. Similar to r, r_s is in the interval [-1,1] and $r_s = 0$ implies no monotonic dependence.

Finally, partial correlation is used when investigating ELMs from different plasmas. Partial correlation measures the degree of association between two random variables while correcting for the effect of another variable, or several other variables, on this relation. The partial correlation of X and Y, adjusted for Z is:

$$\rho_{XYZ} = \frac{\rho_{XY} - \rho_{XZ}\rho_{YZ}}{\sqrt{(1-\rho_{XZ}^2)(1-\rho_{YZ}^2)}}. \tag{8}$$

Partial correlation can also be computed for Spearman's rank correlation coefficient.

3. Analysis of the relation between ELM properties

The relation between W_{ELM} and Δt_{ELM}, averaged over all ELMs in a single discharge, is shown in figure 6(a) and (b) for ILW and CW plasmas, respectively. In agreement with the findings in [18], there is a strongly positive correlation between W_{ELM} and Δt_{ELM} for ILW plasmas as well as for CW plasmas. Likewise, as shown in figure 6 (c) and (d) there is a strong linear relationship between average relative ELM energy loss $\bar{W}_{ELM}/\bar{W}_{tot}$ and Δt_{ELM}. However, ELM control is targeted at influencing the energy loss of individual ELMs. Thus, basing the mitigation strategy on the relation between the average properties of different plasmas can possibly be an oversimplification. Furthermore, the relation presented in [18] does not take into account the uncertainty on W_{ELM} and Δt_{ELM}. Nevertheless, it can be observed from figure 7 that the standard deviation of W_{ELM} and Δt_{ELM} is substantial and increases roughly linearly with the mean value. A straightforward extrapolation based on figure 7(b) would suggest 7 - 10 MJ of standard deviation around an absolute W_{ELM} of 20 - 30 MJ at ITER.

In general, the probability distributions of ELM properties contain comprehensive information about their variability [32][33][34] and therefore studying their statistical correlation properties will yield a better insight into the strength of any existing relations. Figure 8 is a reproduction of figure 6, with the addition of the error bars indicating a single standard deviation. The strongly linear relations depicted in figure 6 appear to be less clear with the inclusion of standard deviations in figure 8. Hence, as will be shown below, the effect of the spread in W_{ELM} and Δt_{ELM} within each plasma is better quantified by studying the relation between W_{ELM} and Δt_{ELM} for individual

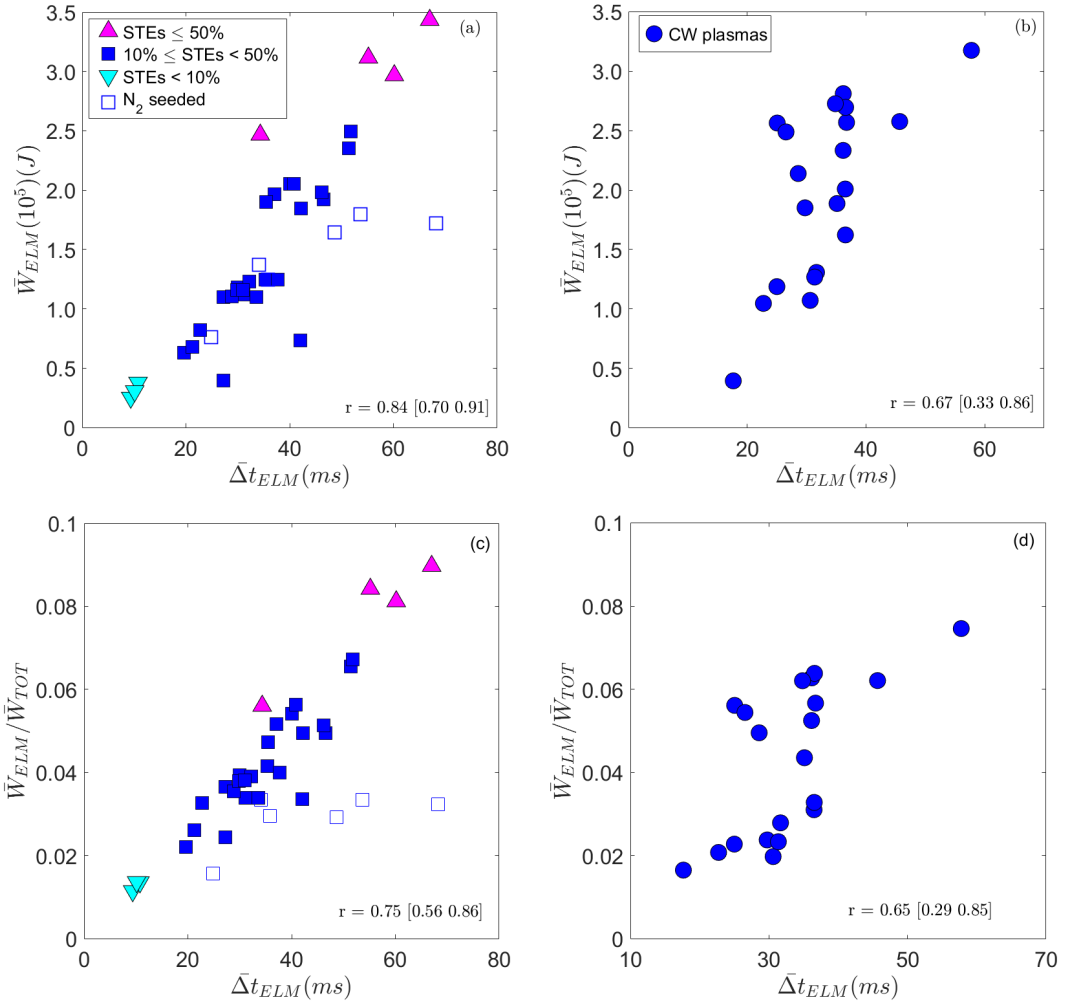

Figure 6. Scatter graphs between $\bar{W}_{ELM}$ and $\bar{\Delta}t_{ELM}$ for (a) JET ILW plasmas, (b) JET CW plasmas. Estimates for the Pearson correlation coefficient (r) are indicated, together with the 95% confidence interval.

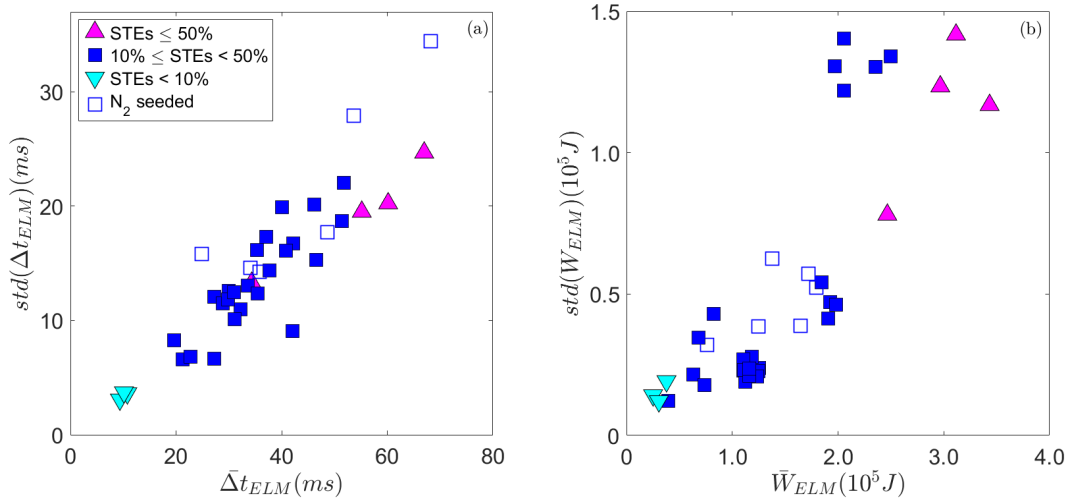

Figure 7. Scatter graphs between mean and standard deviation of (a) Δt_{ELM} and (b) W_{ELM}, for the JET ILW plasmas.

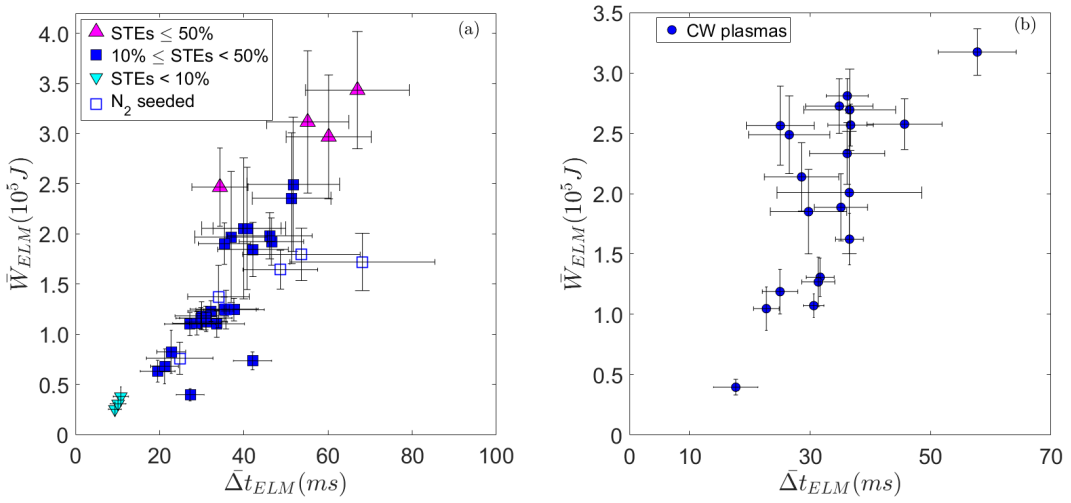

Figure 8. Scatter graphs between $\bar{W}_{ELM}$ and $\bar{\Delta}t_{ELM}$, including the error bars specified by a single standard deviation, for (a) JET ILW plasmas, (b) JET CW plasmas.

ELMs in a discharge. Furthermore, the relation between $\bar{W}_{ELM}$ and $\bar{\tau}_{ELM}$ for ILW and CW plasmas is shown in figure 9 (a)-(b). The correlation is clearly different in the two cases: ILW plasmas exhibit a strongly positive correlation, whereas CW plasmas appear to have no correlation. Further, the correlation coefficient r for the CW plasmas does not reject the null hypothesis of zero correlation at 5 percent significance level. This provides a quantitative affirmation of a lack of correlation. As a next step, the correlation between $\bar{W}_{ELM}/\bar{W}_{tot}$ and $\bar{\tau}_{ELM}$ is examined in figure 9 (c)-(d). This too reveals a trend in correlation similar to that observed in figure 9 (a)-(b). Next, the ILW plasmas are split into two groups and the correlation analysis is performed on each group separately. As indicated in figure 9(c), the first group comprises of plasmas with $\bar{\tau}_{ELM} \leq 4ms$ and the second group consists of plasmas with $\bar{\tau}_{ELM} > 4ms$. The plasmas in the first group have $\bar{\tau}_{ELM}$ comparable to the $\bar{\tau}_{ELM}$ of the CW plasmas analysed in this work whereas the plasmas in the second group have a relatively high f_{STE} and $\bar{\tau}_{ELM}$ greater than the $\bar{\tau}_{ELM}$ of the analysed CW plasmas. It can be noted from figure 9(c) that each of the two groups exhibit a high correlation between $\bar{W}_{ELM}/\bar{W}_{tot}$ and $\bar{\tau}_{ELM}$. The high correlation exhibited by the first group of ILW plasmas indicates that strong correlation between $\bar{W}_{ELM}$ and $\bar{\tau}_{ELM}$ cannot be fully attributed to the presence of STEs in the ILW plasmas.

3.1. Properties of individual ELMs

After studying the ELM properties averaged over a window of stationary plasma conditions, we now concentrate on relations between the properties of the individual ELMs. Estimates of the correlation between W_{ELM} and Δt_{ELM} ($r_{\Delta t_{ELM}-W_{ELM}}$), along with 95% confidence intervals are presented in figure 10 and figure 11 for individual ELMs in JET ILW and JET CW plasmas, respectively. Despite $\bar{W}_{ELM}$ and

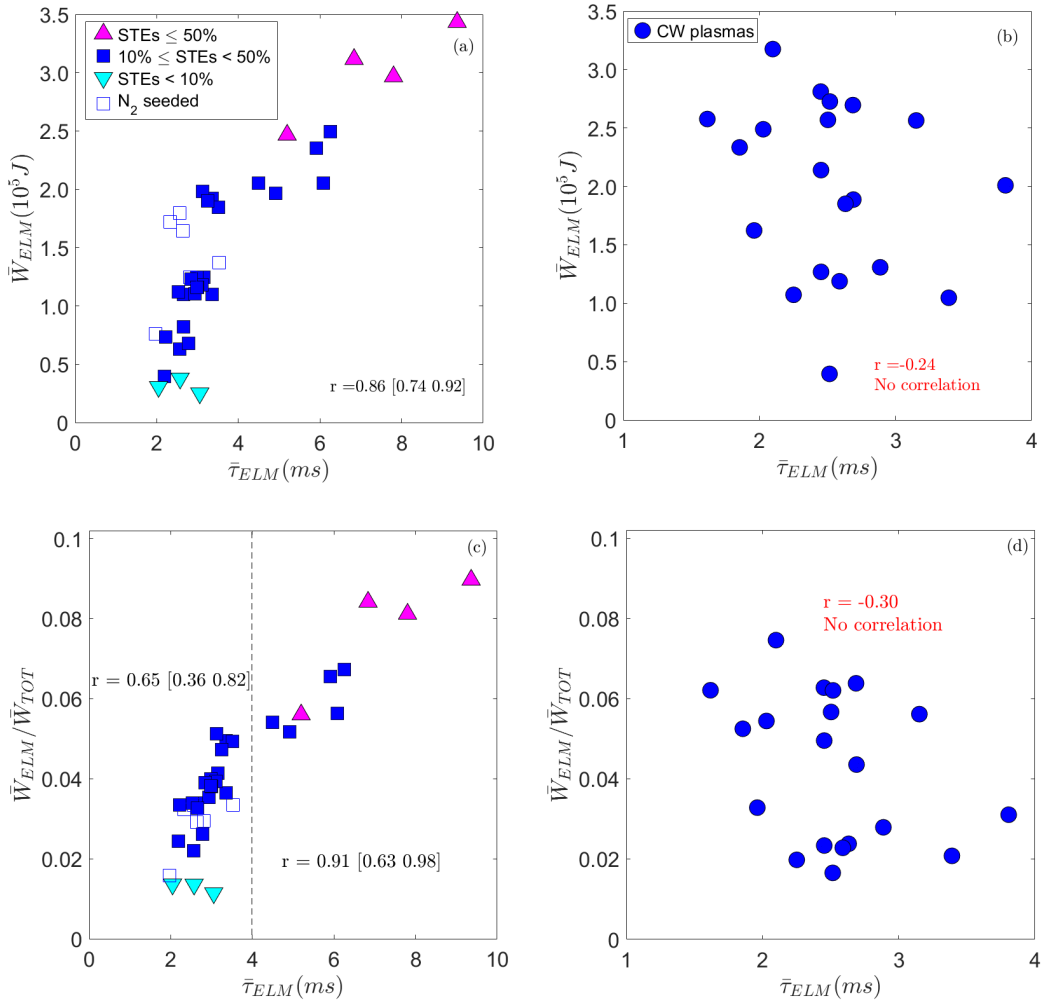

Figure 9. Scatter graphs between $\bar{W}_{ELM}$ and $\bar{\tau}_{ELM}$ for (a) JET ILW plasmas, (b) JET CW plasmas. Scatter graphs between $\bar{W}_{ELM}/\bar{W}_{tot}$ and $\bar{\tau}_{ELM}$ for (a) JET ILW plasmas, (b) JET CW plasmas. Estimates for the Pearson correlation coefficient (r) are indicated, together with the 95% confidence interval. In (c) r values for the two groups of ILW plasmas ($\bar{\tau}_{ELM} \leq 4ms$ and $\bar{\tau}_{ELM} > 4ms$) are indicated. CW plasmas, in contrast to ILW plasmas, do not reject the null hypothesis of zero correlation at 5% significance level.

$\bar{\Delta}t_{ELM}$ conforming to the expected inverse dependence between W_{ELM} and f_{ELM}, the correlation between W_{ELM} and Δt_{ELM} for individual ELMs varies from being strongly correlated for certain plasmas to being uncorrelated for others. This is observed in both CW as well as ILW plasmas. Compared to ILW discharges, CW plasmas on the whole have higher correlation between W_{ELM} and Δt_{ELM} for individual ELMs, with 12 out of the 20 (60%) analyzed plasmas exhibiting high correlation ($r > 0.40$) and 4 out of the 20 (20%) analyzed plasmas demonstrating no correlation ($r \leq 0.20$). On the other hand, out of the 38 ILW plasmas, only the 6 (16%) N_2-seeded plasmas exhibit high correlation ($r > 0.40$), whereas 19 (50%) plasmas show no correlation and 13 (34%) have a medium correlation.

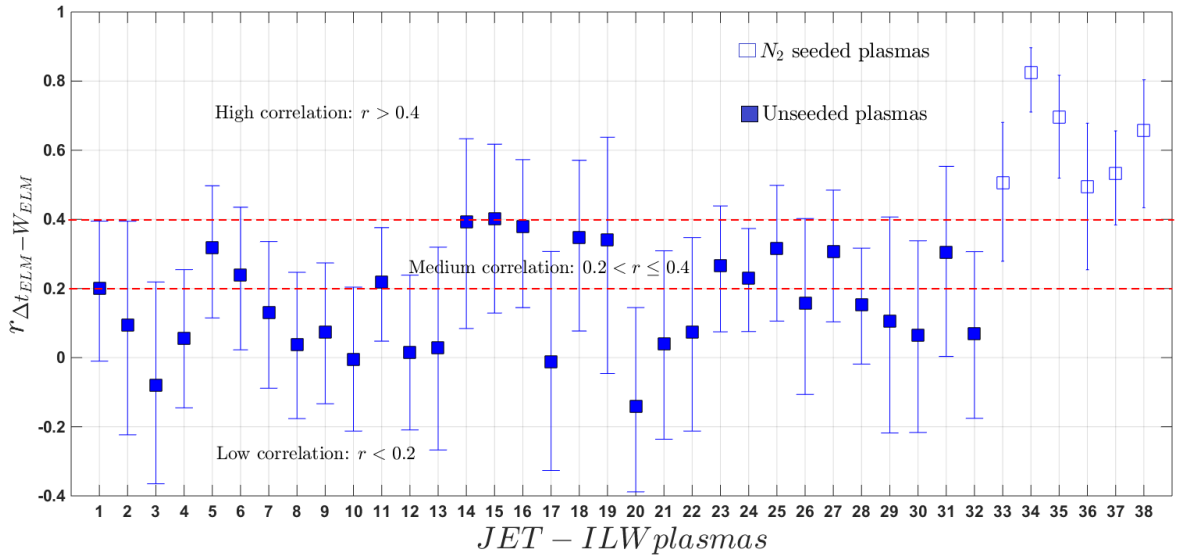

Figure 10. Estimates of linear correlation between W_{ELM} and Δt_{ELM} for individual ELMs in JET ILW plasmas. 95% confidence intervals are also indicated. Discharges indexed 33 to 38 are N_2-seeded plasmas.

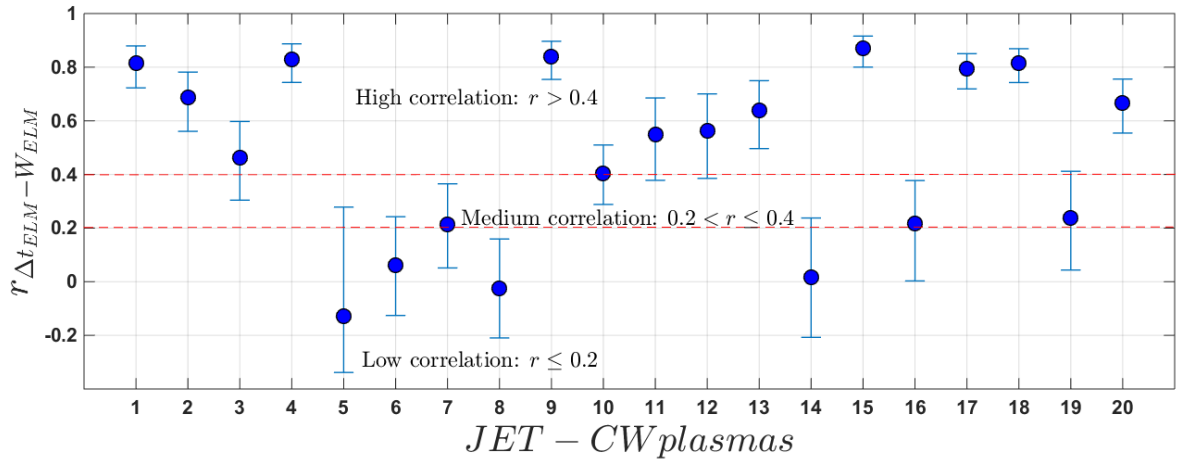

Figure 11. Estimates of linear correlation between W_{ELM} and τ_{ELM} for individual ELMs in JET CW plasmas. 95% confidence intervals are also indicated.

The underlying processes causing W_{ELM} and Δt_{ELM} to exhibit varying degrees of correlation could be one or several of the following. The size of W_{ELM} is controlled by the pedestal parameters, i.e. the density and temperature inside the pedestal before the ELM crash [35][36]. A multi-machine study performed on ASDEX, DIII-D, JT60U and JET CW has established that the relative ELM energy losses scale with the inverse of pedestal collisionality [35]. Other key parameters that have an important effect on W_{ELM} are the pedestal width [37], plasma rotation [38] and the plasma shape [39]. On the other hand, Δt_{ELM} is a consequence of the various timescales involved in the recovery of the pedestal to its pre-ELM state following the ELM crash. The pedestal recovery

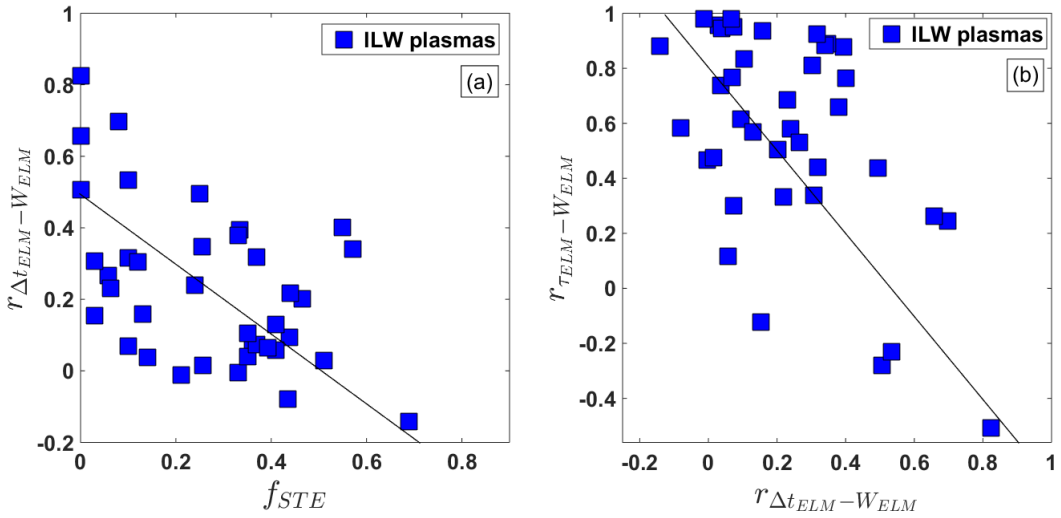

Figure 12. Variation of linear correlation between W_{ELM} and Δt_{ELM} ($r_{(\Delta t_{ELM})-W_{ELM})}$) for individual ELMs in JET ILW plasmas. (a) With the fraction of slow transport events (f_{STE}) and (b) with the linear correlation between W_{ELM} and τ_{ELM} ($r_{(\tau_{ELM}-W_{ELM})}$) for individual ELMs in JET ILW plasmas.

time can be potentially modified by enhanced losses in the inter-ELM period, either by increased bulk radiation or by an increased level of density and magnetic fluctuations. W_{ELM}, being determined primarily by the pre-ELM pedestal plasma parameters, is likely to remain unaffected by the inter-ELM processes that can potentially modify Δt_{ELM}. Furthermore, the peeling-ballooning model, which is a leading candidate for explaining ELM onset, fails to explain the phase of saturated gradients without ELMs [40]. In medium-sized tokamaks at low edge temperature, the bootstrap current seems to be fully developed for a relatively long time interval before an ELM crash. It is reasonable to assume that, after the pedestal has recovered, an additional increase in Δt_{ELM} will not lead to an additional increase in W_{ELM}. Finally, figure 12 suggests that, in the case of the ILW plasmas, the correlation between W_{ELM} and Δt_{ELM} for individual ELMs varies inversely with f_{STE}. Hence, the presence of the STEs appears to be at least partly responsible for the observed reduction in correlation between ELM waiting times and energies in ILW plasmas.

Furthermore, we note that for ILW plasmas there is a weakly inverse relation between the correlation among W_{ELM} and Δt_{ELM} and the correlation among τ_{ELM} and W_{ELM}. It can be seen from figure 12 that plasmas with high f_{STE} exhibit no correlation between W_{ELM} and Δt_{ELM} and consequently a very high correlation between τ_{ELM} and W_{ELM}. As an illustration, scatter plots between W_{ELM} and Δt_{ELM} and W_{ELM} and τ_{ELM} for three representation plasmas are given in figure 13. On the one hand, non-seeded JET-ILW plasma #82806 with $f_{STE} \geq 0.5$ exhibits a very high correlation between W_{ELM} and τ_{ELM} and no correlation between W_{ELM} and Δt_{ELM}. On the other hand, N_2-seeded JET-ILW plasma #83179, similar to JET-CW plasma #76479, demonstrates a high correlation between W_{ELM} and Δt_{ELM} and no correlation between W_{ELM} and

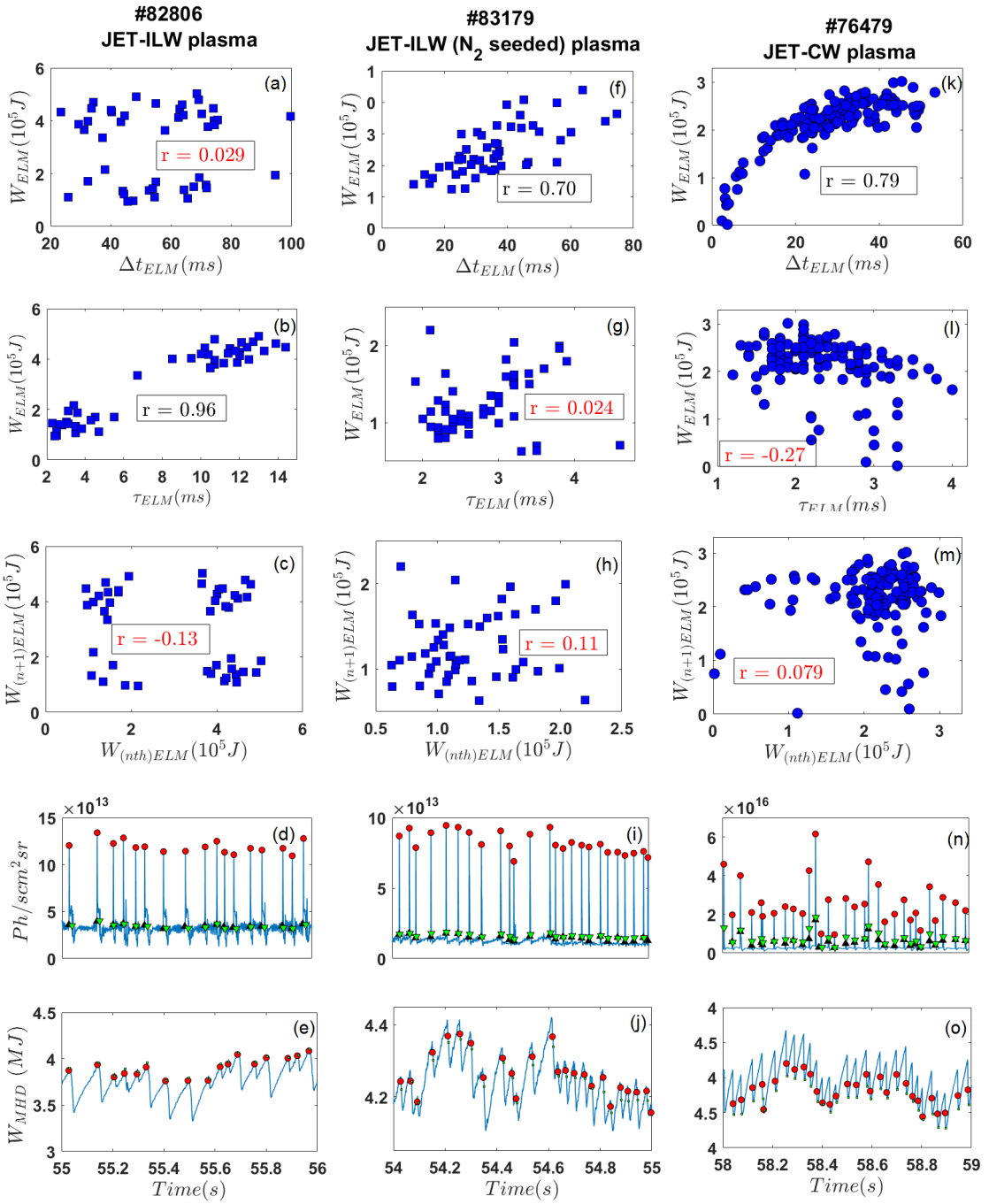

Figure 13. Scatter plot between W_{ELM} and Δt_{ELM}, W_{ELM} and τ_{ELM} and $W_{(nth)ELM}$ and $W_{(n+1)ELM}$ for (a)-(c). JET pulse #82806 (unseeded JET ILW plasma ($STEs > 50\%$)), (f)- (h). #83179 (N_2-seeded JET ILW plasma) and (k)-(m). #76479 (JET CW plasma). Estimates of r for each scatter plot are also specified. r estimates that do not reject the hypothesis of no correlation at 5% significance level are indicated in color red. Also given are time traces of Be II radiation from the inner divertor (ILW plasmas), D_α from the inner divertor (CW plasma) and the equilibrium stored energy (W_{MHD}).

τ_{ELM}.

3.2. Collective properties of individual ELMs in all analyzed plasmas

Next, the collective properties of all ELM events in our JET ILW database are investigated. A scatter diagram between W_{ELM} and Δt_{ELM} for all ELMs (excluding N_2-seeded plasmas) is shown in figure 14(a). Table 4 lists the estimates for r and r_s corresponding to the scatter diagram presented in figure 14(a). Partial correlations between W_{ELM} and Δt_{ELM}, while controlling for B_t, I_p, P_{input}, n_e, Γ_{D_2} and δ_{avg}, are presented as well. In this case partial correlation is a more realistic measure for assessing the relation between W_{ELM} and Δt_{ELM}, since it takes into account the widely varying global plasma conditions across the data set. It is noteworthy that adjusting for the varied plasma conditions brings a significant reduction in the correlation. Moreover, values of r_s are comparable with r, which confirms the robustness of r estimates.

Furthermore, in order to account for any variation of the standard deviation of the data (heteroscedasticity), which is especially clear in figure 14(a) (see also figure 7), a scatter diagram between the logarithm of W_{ELM} and Δt_{ELM} for all ELMs in the analyzed ILW plasmas (excluding N_2-seeded plasmas) is shown in figure 14(b). Also, on figure 14(b), the least-squares line of best fit is indicated and the corresponding regression coefficients are given in table 5. The observed linearity in the log-log space is indicative of a power law relation between W_{ELM} and Δt_{ELM}. This implies that the rate of change of W_{ELM} and Δt_{ELM} decreases gradually up to a point beyond which the two quantities become almost independent. This is reaffirmed by the inspection of figure 14(a) where there appears to be a saturation of W_{ELM} for Δt_{ELM} greater than 25-30 ms. This is also in agreement with an earlier observation of statistical independence between W_{ELM} with Δt_{ELM} beyond $\Delta t_{ELM} = 20ms$, made by Webster *et al.* [19] for individual ELMs from a set of $2T$, $2MA$ JET ILW plasmas. The point beyond which W_{ELM} becomes independent of Δt_{ELM} is likely to be limited by the pedestal recovery time and the total energy stored in the plasma. In the plasmas considered in this work, although the plasma thermal energy for pure ELMs appears to increase until the next ELM, it is largely recovered to its pre-ELM value in $25(\pm 8)ms$. This suggests a scenario in which the edge pedestal is largely restored in $\approx 25ms$, leading to a significant reduction in the correlation between W_{ELM} for Δt_{ELM} beyond $\Delta t_{ELM} \approx 25ms$. On the other hand, for ELMs followed by STEs, the plasma thermal energy recovers to its pre-ELM+STE value in $90(\pm 10)ms$. Furthermore, it can be estimated that for ILW ELMs a reduction of

Table 4. Estimates of regular and partial correlations, based on Pearson (r) and Spearman (r_s) coefficients, between W_{ELM} and Δt_{ELM} for all ELMs in the JET ILW plasmas. The partial correlations control for B_t, I_p, P_{input}, n_e, Γ_{D_2} and δ_{avg}.

	r	r_s
Regular	0.58	0.65
Partial	0.21	0.26

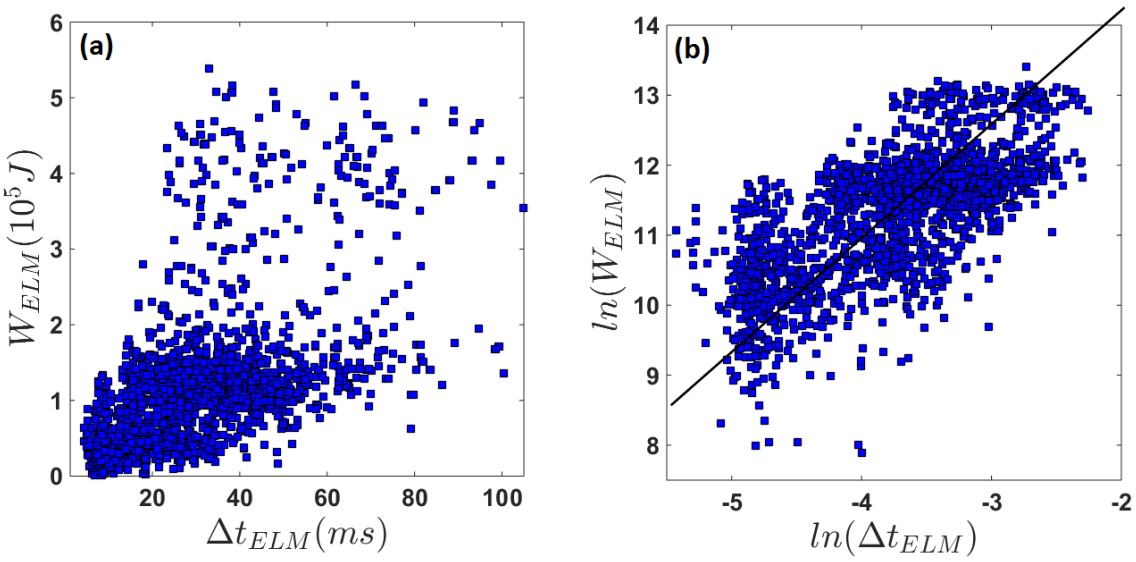

Figure 14. Scatter graph between (a) W_{ELM} and Δt_{ELM}, (b) Logarithm of W_{ELM} and Δt_{ELM} for all ELMs in JET ILW plasmas. The least-squares line of best fit to the logarithm of W_{ELM} and Δt_{ELM} is also shown.

Table 5. Estimated coefficients and standard errors for the least-squares line of best fit shown in figure 14(b). The *model* is $ln(W_{ELM}) = \beta_0 + \beta_1 ln\Delta t_{ELM}$.

β_0	β_1	SE_{β_0}	SE_{β_1}
14.7	0.895	0.071	0.019

Δt_{ELM} from 25-30 ms (beyond which W_{ELM} and Δt_{ELM} are very weakly correlated) to 10 ms reduces W_{ELM} by $\approx 60\%$. On the other hand, a reduction of Δt_{ELM} from 50-60 ms to 25-30 ms, reduces W_{ELM} by $\approx 40\%$. This suggests that if ELMs are consistently paced at 10 ms, W_{ELM} can be reduced by $\approx 60 - 70\%$.

4. Global dependence of correlation between ELM energy losses and waiting times

Since the success of ELM mitigation depends considerably on a high correlation between W_{ELM} and Δt_{ELM}, we now aim to locate the regions of plasma operational space where the corresponding correlation coefficient $r_{(\Delta t_{ELM} - W_{ELM})}$ is large. One approach for studying the dependence of $r_{(\Delta t_{ELM} - W_{ELM})}$ on plasma parameters would be to rely on single parameter scans. In the case of the present work, there are not enough dedicated experiments available to allow such a study. Nevertheless, as a preliminary step, in figure 15 and figure 16 scatter plots between the plasma engineering parameters B_t, I_p, P_{input}, n_e, Γ_{D_2}, δ_{avg} and the correlation coefficient $r_{(\Delta t_{ELM} - W_{ELM})}$ are provided. It can be observed that individually none of the plasma engineering parameters discriminate well between plasmas with a high, medium or zero $r_{(\Delta t_{ELM} - W_{ELM})}$. As a next step, regression

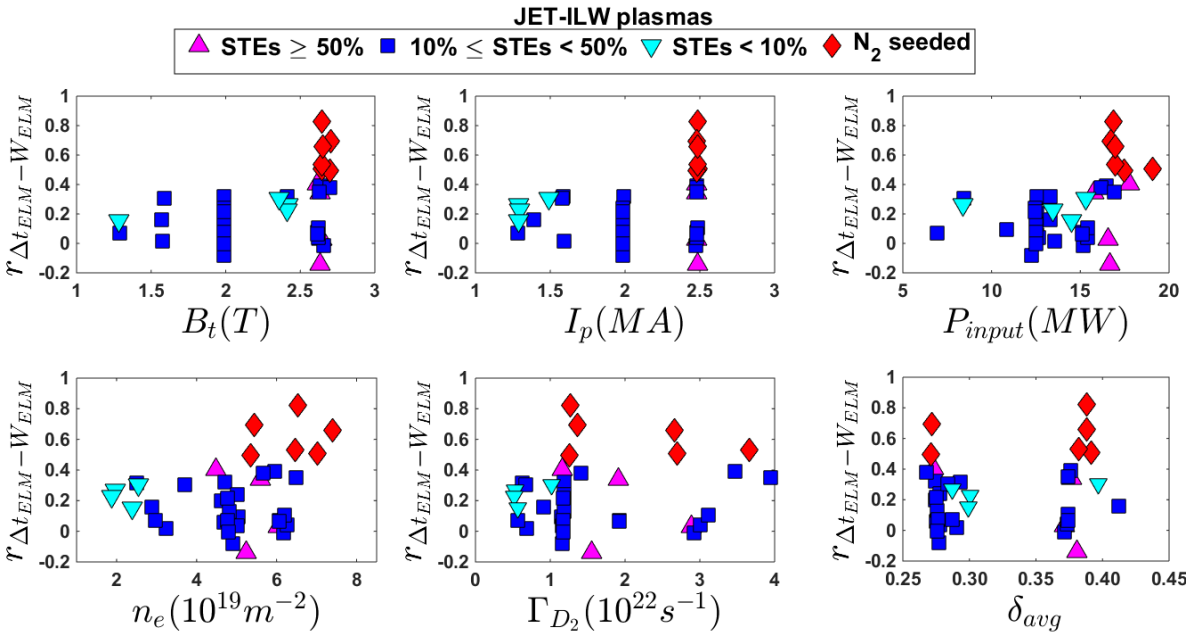

Figure 15. Scatter plots of correlation between W_{ELM} and Δt_{ELM} ($r_{(\Delta t_{ELM}-W_{ELM})}$) and plasma engineering parameters B_t, I_p, P_{input}, n_e, Γ_{D_2} and δ_{avg} for JET ILW plasmas.

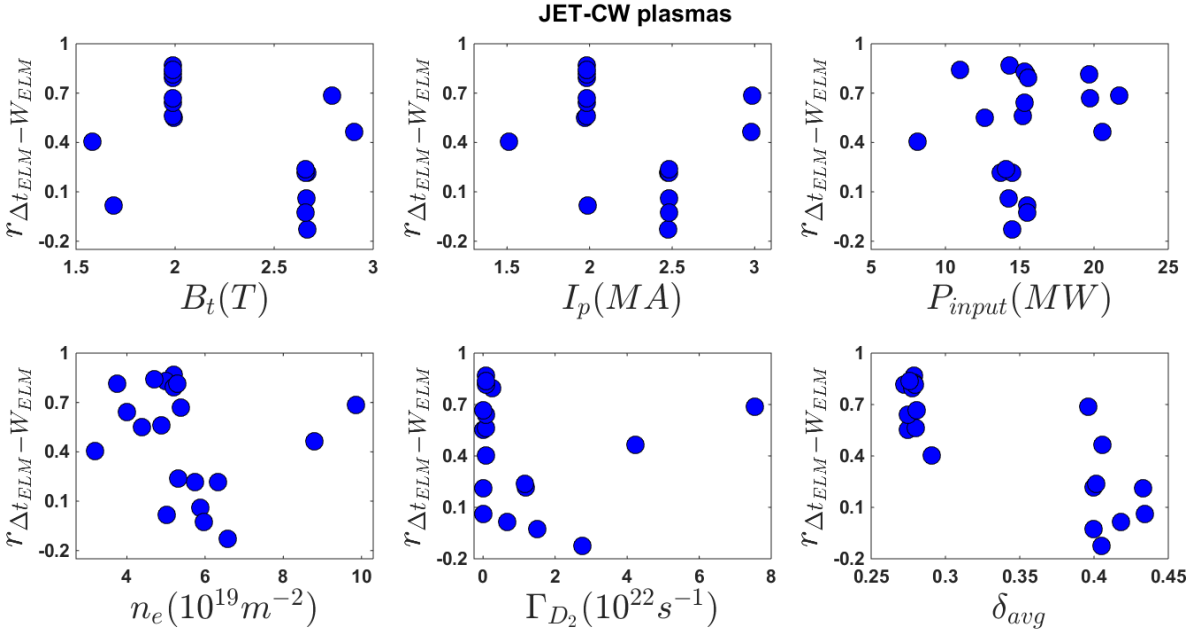

Figure 16. Scatter plots of correlation between W_{ELM} and Δt_{ELM} ($r_{(\Delta t_{ELM}-W_{ELM})}$) and plasma engineering parameters B_t, I_p, P_{input}, n_e, Γ_{D_2} and δ_{avg} for JET CW plasmas.

analysis is used for quantifying the effect of plasma parameters on $r_{(\Delta t_{ELM}-W_{ELM})}$. As discussed in section 2.4, the sampling distribution of r is not normal, therefore r is transformed to the quantity z in (5). Standard multilinear regression using least squares is then performed for yielding the regression coefficients given in table 6. Standard error (SE) of the regression coefficients is also given in table 6.

The regression model for CW plasmas is constructed using B_t, I_p,P_{input},n_e, Γ_{D_2} and δ_{avg} as predictor variables. For ILW plasmas, however, f_{STE} is included as an additional predictor variable, as it has been shown in section 3.1 that f_{STE} has an appreciable influence on $r_{(\Delta t_{ELM}-W_{ELM})}$. In addition, since f_{STE} is not strictly an engineering quantity, a second model (model 2) for ILW plasmas is constructed using Γ_{N_2} as an additional parameter in place of f_{STE}. The quality of the fitted regression model is quantified with the root-mean-square error (RMSE(%)), which is an indicator of the deviation of the measurements from the model, and the coefficient of determination ($R^2 \in [0,1]$), which measures the degree to which the predictor variables and the regression model explain the observed variation of the response variable. Based on the values of RMSE and R^2, each model is fairly appropriate to describe the variation of the correlation.

It is noteworthy that a direct comparison between the regression coefficients of different parameters cannot be made as they are measured on different scales. However, an examination of the standard errors of the coefficients indicate the parameters that contribute most to the regression model. Across both model 1 and model 2 that are constructed for ILW plasmas, f_{STE} or alternatively Γ_{N_2} appear to be the most important determinant of $r_{(\Delta t_{ELM}-W_{ELM})}$ as their coefficient estimates are much greater than the SEs. This is expected since it has earlier been noted in section 3.1 that it is only with N_2 seeding that high values of $r_{(\Delta t_{ELM}-W_{ELM})}$ comparable with CW plasmas are obtained. In unseeded ILW plasmas the correlation fluctuates at most to a weakly positive correlation from a state of no correlation. Secondary to f_{STE}/Γ_{N_2}, Γ_{D_2} emerges as the more important determinant of $r_{(\Delta t_{ELM}-W_{ELM})}$. This is consistent with the model for CW plasmas as therein δ_{avg} followed by Γ_{D_2} appear to be the most important of the considered plasma engineering parameters. For the remaining parameters it can be noted that SE is comparable and sometimes slightly higher than the coefficient estimate which suggests that they are less contributory to the regression model.

It is important to note that in addition to the global time-averaged plasma engineering parameters, the regression models could substantially benefit if the complete distributions of the predictor parameters would be considered.

5. Relation between energy loss of successive ELMs

Finally, the relationship between energy losses of consecutive ELMs is investigated. As can be noted from table 7, only 10 - 15 percent of the analyzed JET-ILW (including N_2-seeded plasmas) and JET-CW plasmas exhibit a weak non-zero correlation. Also, the values of r_s are in agreement with estimates of r. W_{ELM} of consecutive ELMs is

Table 6. Least-squares multilinear regression fits (including a cut-off term C) for correlation between W_{ELM} and Δt_{ELM} using global plasma parameters as predictors. The coefficient estimate alongside 95% confidence intervals are presented, together with the root-mean-square error (RMSE) and the coefficient of determination (R^2).

	CW		**ILW**			
			Model 1		**Model 2**	
	Coeff	SE	Coeff	SE	Coeff	SE
C	1.67	0.58	-0.457	0.30	0.0287	0.29
$B_t(T)$	-0.982	0.64	0.0483	0.17	0.162	0.15
$I_p(MA)$	1.62	1.06	0.559	0.48	0.0791	0.38
$P_{input}(MW)$	-0.0229	0.031	0.0119	0.024	0.0080	0.022
$n_e(10^{19}m^{-2})$	0.165	0.13	-0.0259	0.10	-0.0486	0.099
$\Gamma_{D_2}(10^{22}s^{-1})$	-0.113	0.070	-0.114	0.075	-0.0422	0.062
δ_{avg}	-8.54	1.5	-0.313	0.90	-0.618	0.85
f_{STE}	–		-1.19	0.27	–	
$\Gamma_{N_2}(10^{22}s^{-1})$	–		–		0.269	0.053
RMSE(%)	23.4		18.3		17.4	
R^2	0.83		0.64		0.67	

Table 7. Number of ILW plasmas (including N_2-seeded plasmas) and CW plasmas with correlation between energy loss of successive ELMs $r > 0.3$, $0.1 < r \leq 0.3$ and $-0.3 < r \leq 0.1$. The number of plasmas with r significantly different from zero are also indicated at two significance levels α.

Plasmas	$-0.3 < r \leq 0.1$	$0.1 < r \leq 0.3$	$r > 0.3$	$r \neq 0$ ($\alpha = 5\%$)	$r \neq 0$ ($\alpha = 1\%$)
ILW	20	15	3	4	2
CW	16	4	0	3	0

largely uncorrelated. This implies that an ELM with a large W_{ELM} is equally likely to be followed by an ELM with a large or small W_{ELM}. Further, this observation is consistent across unseeded JET-ILW plasmas, N_2-seeded JET-ILW plasmas and JET-CW plasmas. This can also be observed in the scatter plots of W_{ELM} of nth ELM and W_{ELM} of $(n+1)th$ ELM in figure 13. For each of the three representative plasmas, #82806, #83179 and #76479, W_{ELM} of successive ELMs is uncorrelated.

6. Conclusions

This work examines the relation between W_{ELM} and Δt_{ELM} for individual ELMs in a set of non-seeded JET-ILW plasmas and compares the results with a set of N_2-seeded JET-ILW plasmas and JET-CW plasmas. It is found that the empirically established inverse relation between average f_{ELM} and $\bar{W}_{ELM}$ is not ubiquitously obeyed by individual ELMs. The linear correlation between W_{ELM} and Δt_{ELM} varies from being strongly correlated for certain plasmas to being completely uncorrelated for others. CW plasmas, in general, exhibit higher correlation between W_{ELM} and Δt_{ELM} than ILW plasmas and it is only in N_2-seeded ILW plasmas that a high correlation comparable to certain CW

plasmas is observed.

Furthermore, ELMs in non-seeded JET ILW plasmas are often followed by a slow transport event resulting in a bi-modal distribution of ELM durations. The two modes correspond to two distinct underlying phenomena: pure ELMs and ELMs followed by a slow transport event. Slow transport events are not present in JET-CW plasmas and they disappear in N_2-seeded JET-ILW plasmas, giving rise to a unimodal asymmetric distribution of ELM durations. The average ELM energy loss in a plasma scales linearly with the proportion of ELMs followed by slow transport events in a plasma, whereas the linear correlation between W_{ELM} and Δt_{ELM} varies inversely with the fraction of slow transport events.

A collective analysis of all the ELMs from the unseeded JET-ILW ELMs plasmas revealed that the variation between W_{ELM} and Δt_{ELM} obeys a power law relationship. W_{ELM} appears to saturate for $\Delta t_{ELM} \approx 25 - 30ms$ which is roughly the time taken for the plasma thermal energy to return to its pre-ELM value. This suggests a scenario where the linear correlation between W_{ELM} and Δt_{ELM} significantly reduces as the edge pedestal recovers to its pre-ELM value.

Moreover, least squares linear regression has been employed for determining the region of the plasma operating regime where the correlation between W_{ELM} and Δt_{ELM} is maximized. A regression model is constructed using plasma and engineering parameters for both JET-ILW and JET-CW plasmas. While the models will certainly benefit from more informative predictors, they nevertheless indicate the more important parameters from the plasma parameters used as predictors. For the JET-ILW plasmas, Γ_{N_2} followed by δ_{avg} and Γ_{D_2} contribute most to the correlation between W_{ELM} and Δt_{ELM}. Similarly, for JET-CW plasmas δ_{avg} and Γ_{D_2} appear to be the most important determinants of correlation.

Lastly it is acknowledged that W_{ELM} and Δt_{ELM} are stochastic quantities and a precise analysis of these quantities needs to effectively incorporate the uncertainty on these quantities. It has also been shown that the standard deviation of W_{ELM} and Δt_{ELM} increases linearly with the mean value. Analyzing W_{ELM} and Δt_{ELM} for individual ELMs subtly allows for the standard deviation in W_{ELM} and Δt_{ELM} to be accommodated and indeed reveals additional information. It is emphasized that analyzing complete probability distributions of W_{ELM}, Δt_{ELM}, τ_{ELM} and other plasma parameters will yield a more comprehensive picture and will thus form the basis of future investigations.

Acknowledgement

This work has been carried out within the framework of the EUROfusion Consortium and has received funding from the EURATOM research and training programme 2014-2018 under grant agreement No 633053. The views and opinions expressed herein do not necessarily reflect those of the European Commission. The authors would like to thank Dr. Lorenzo Frassinetti for his useful feedback on this work.

References

[1] Zohm H 1996 Edge-localized modes (ELMs) *Plasma Phys. Control. Fusion* **38** 2 105

[2] Wesson J 2011 *Tokamaks* 4th ed Oxford University Press

[3] Lang PT *et al* 2013 ELM control strategies and tools: status and potential for ITER *Nucl. Fusion* **53** 043004

[4] Brezinsek S 2015 Plasma-surface interaction in the Be/W environment: Conclusions drawn from the JET-ILW for ITER *J. Nucl. Mater.* **463** 11-21

[5] Evans T 2013 ELM mitigation techniques *J. Nucl. Mater.* **438** S11-18

[6] Eich T *et al* 2016 ELM divertor heat load scaling to ITER with data from JET, ASDEX Upgrade and MAST *22nd International Conference on Plasma Surface Interactions in Controlled Fusion Devices*

[7] Eich T *et al* 2011 Type-I ELM power deposition profile width and temporal shape in JET *J. Nucl. Mater.* **415** S856-59

[8] Jakubowski MW *et al* 2009 Overview of the results on divertor heat loads in RMP controlled H-mode plasmas on DIII-D *Nucl. Fusion* **49** 9

[9] Thomsen H *et al* 2011 Power load characterization for type-I ELMy H-modes in JET *Nucl. Fusion* **51** 123001

[10] Loarte A *et al* 2014 Progress on the application of ELM control schemes to ITER scenarios from the non active phase to DT operation *Nucl. Fusion* **54** 033007

[11] Bortolon A *et al* 2016 High frequency pacing of edge localized modes by injection of 455 lithium granules in DIII-D H-mode discharges *Nucl. Fusion* **56** 056008

[12] de la Luna E *et al* 2016 Understanding the physics of ELM pacing via vertical kicks in JET in view of ITER *Nucl. Fusion* **56** 026001

[13] Kallenbach A *et al* 2005 Tokamak operation with high-Z plasma facing components *Plasma Phys. Control. Fusion* **47** 12B

[14] Neu R *et al* 2013 First operation with the JET International Thermonuclear Experimental Reactor-like wall *Phys. Plasmas* **20** 5 056111

[15] Dux R, Janzer A, Puetterich T and ASDEX Upgrade Team 2011 Main chamber sources and edge transport of tungsten in H-mode plasmas at ASDEX Upgrade *Nucl. Fusion* **51** 053002

[16] Lang PT *et al* 2003 ELM frequency control by continuous small pellet injection in ASDEX Upgrade *Nucl. Fusion* **43** 10 1110-1120

[17] Liang Y 2011 Overview of Edge Localized Modes Control in Tokamak Plasmas *Fusion Sci. Technol.* **59** 3 586-601

[18] Herrmann A 2002 Overview on stationary and transient divertor heat loads *Plasma Phys. Control. Fusion* **44** 6 883-903

[19] Webster AJ, Webster SJ and JET-EFDA contributors 2014 Processes and properties of edge-localized instabilities in 2T 2MA plasmas in the Joint European Torus *Phys. Plasmas* **21** 11 112502

[20] Beurskens M *et al* 2014 Global and pedestal confinement in JET with a Be/W metallic wall *Nucl. Fusion* **54** 4 043001

[21] Giroud C *et al* 2013 Impact of nitrogen seeding on confinement and power load control of a high-triangularity JET ELMy H-mode plasma with a metal wall *Nucl. Fusion* **53** 11 113025

[22] Frassinetti L *et al* 2015 Effect of nitrogen seeding on the energy losses and on the time scales of the electron temperature and density collapse of type-I ELMs in JET with the ITER-like wall *Plasma Phys. Control. Fusion* **55** 2 023007

[23] Frassinetti L *et al* 2016 ELM behavior in ASDEX Upgrade with and without nitrogen seeding *Plasma Phys. Control. Fusion* **57** 2 022004

[24] Schneider PA *et al* 2015 Pedestal and edge localized mode characteristics with different first wall materials and nitrogen seeding in ASDEX Upgrade *Plasma Phys. Control. Fusion* **57** 1 014029

[25] Wiesen S *et al* 2016 Effect of PFC Recycling Conditions on JET Pedestal Density *Contrib.*

Plasma Phys **56** No.6-8 754-759
[26] Brezinsek S *et al* 2016 Characterisation of the deuterium recycling at the W divertor target plates in JET during steady state plasma conditions and ELMs *Phys. Scripta* **T167** 014076
[27] Ngatchou-Wandji J 2006 On Testing for the Nullity of Some Skewness Coefficients *Int. Stat. Rev.* **74** 1 47-65
[28] Gibbons JD and Chakraborti S 2010 *Nonparametric Statistical Inference* 5th ed Chapman and Hall
[29] Lehmann EL and Romano JP 2005 *Testing Statistical Hypothesis* 3rd ed Springer
[30] O. Kardaun 2005 Classical methods of statistics, Springer.
[31] Johnson NL, Kotz S and Balakrishnan N 1995 *Continuous Univariate Distributons* 2nd ed John Wiley & Sons
[32] Shabbir A, Verdoolaege G, Kardaun OJWF, Noterdaeme JM and JET-EFDA contributors 2014 Visualization of the operational space of edge-localized modes through low-dimensional embedding of probability distributions *Rev. Sci. Instrum.* **85** 11 11E819
[33] Verdoolaege G, Karagounis G, Tendler M and Van Oost G 2012 Pattern recognition in probability spaces for visualization and identification of plasma confinement regimes and confinement time scaling *Plasma Phys. Control. Fusion* **54** 12 124006
[34] Shabbir A, Verdoolaege G, Vega J and Murari A 2015 ELM Regime Classification by conformal prediction on an information manifold *IEEE T. Plasma Sci.* **43** 12 4190-4199
[35] Loarte A *et al* 2003 Characteristics of type I ELM energy and particle losses in existing devices and their extrapolation to ITER *Plasma Phys. Control. Fusion* **45** 9 1549-69
[36] Loarte A *et al* 2002 Characteristics and scaling of energy and particle losses during Type I ELMs in JET H-modes *Plasma Phys. Control. Fusion* **44** 9 1815-44
[37] Snyder PB *et al* 2002 Edge localized modes and the pedestal: A model based on coupled peeling ballooning modes *Phys. Plasmas* **9** 5 2037-2043
[38] Oyama N *et al* 2005 Energy loss for grassy ELMs and effects of plasma rotation on the ELM characteristics in JT-60U *Nucl. Fusion* **45** 8 871-81
[39] Osborne T *et al* 2000 The effect of plasma shape on H-mode pedestal characteristics on DIII-D *Plasma Phys. Control. Fusion* **42** 5A A175-84
[40] Zohm H 2014 *Magnetohydrodynamic Stability of Tokamaks* Wiley-Vch